# Neuromorphic meets neuromechanics, Part II: The role of fusimotor drive

# Neuromorphic Meets Neuromechanics, Part II: The Role of Fusimotor Drive

**Kian Jalaleddini**[1], **Chuanxin Minos Niu**[2], **Suraj Chakravarthi Raja**[3], **Won Joon Sohn**[6], **Gerald E. Loeb** [4], **Terence D. Sanger**[3,4,5], **Francisco J. Valero-Cuevas**[1,4]

[1] Division of Biokinesiology and Physical Therapy, University of Southern California, USA.

[2] Department of Rehabilitation, Ruijin Hospital, School of Medicine, Shanghai Jiao Tong University, Shanghai, China.

[3] Department of Electrical Engineering, University of Southern California, USA.

[4] Department of Biomedical Engineering, University of Southern California, USA.

5 Department of Neurology, University of Southern California, USA.

6 Department of Rehabilitation Medicine, Emory University, Atlanta, GA, USA.

E-mail: valero@usc.edu

August 2016

**Abstract.**

**Objective:** We studied the fundamentals of muscle afferentation by building a neuro-mechano-morphic system actuating a cadaveric finger. This system is a faithful implementation of the stretch reflex circuitry. It allowed the systematic exploration of the effects of different fusimotor drives to the muscle spindle on the closed-loop stretch reflex response.

**Approach:** As in Part I of this work, sensory neurons conveyed proprioceptive information from muscle spindles (with static and dynamic fusimotor drive) to populations of $\alpha$-motor neurons (with recruitment and rate coding properties). The motor commands were transformed into tendon forces by a Hill-type muscle model (with activation-contraction dynamics) via brushless DC motors. Two independent afferented muscles emulated the forces of *flexor digitorum profundus* and the *extensor indicis proprius* muscles, forming an antagonist pair at the metacarpophalangeal joint of a cadaveric index finger. We measured the physical response to repetitions of bi-directional ramp-and-hold rotational perturbations for 81 combinations of static and dynamic fusimotor drives, across four ramp velocities, and three levels of constant cortical drive to the $\alpha$-motor neuron pool.

**Results:** We found that this system produced responses compatible with the physiological literature. Fusimotor and cortical drives had nonlinear effects on the reflex forces. In particular, only cortical drive affected the sensitivity of reflex forces to *static* fusimotor drive. In contrast, both static fusimotor and cortical drives reduced the sensitivity to *dynamic* fusimotor drive. Interestingly, realistic signal-dependent motor noise emerged naturally in our system without having been explicitly modeled.

**Significance:**: We demonstrate that these fundamental features of spinal afferentation sufficed to produce muscle function. As such, our neuro-mechano-morphic system is a viable platform to study the spinal mechanisms for healthy muscle function — and its

$\mathLaTeX 2_\varepsilon$                                                                                          2

pathologies such as dystonia and spasticity. In addition, it is a working prototype of a robust biomorphic controller for compliant robotic limbs and exoskeletons.

## 1. INTRODUCTION

The physiology of fusimotor drive encompasses the interaction of $\gamma$-motoneurons with intrafusal muscle fibers. This interaction assists in both set muscle tone and modulation of stretch reflexes. These mechanisms lie at the heart of many theories of motor control because they provide the physiological bases for healthy and pathological muscle function [1]. Yet the functional significance of the specific features and details of fusimotor drive remain poorly understood.

Fusimotor drive is thought to adjust the gain of the feedback in the feedback control hypothesis (e.g., [2–4]), or modify the equilibrium of a limb by shifting the thresholds of stretch reflexes in the equilibrium point hypothesis (e.g., [5, 6]). But what are the physiological mechanisms by which cortico-spinal commands can set these gains or thresholds? Stretch reflexes have also been proposed as a mechanism for sensorimotor pathologies. For instance, spasticity—which is present in multiple conditions such as cerebral palsy, multiple sclerosis, spinal cord injury, stroke, etc.—, is thought to come from hyperexcitability of the stretch reflex pathway and other spinal reflexes (e.g., [7]). But what are the specific spinal, cortical or subcortical pathways, gains or circuits responsible for these dysfunctional responses? And are they common across these conditions? Increased fusimotor drive increases spindle afferent activity in stretched muscles that is thought to contribute to the increased spasticity (e.g., [8]). But what exactly defines the joint angle and angular velocity thresholds for spastic responses? Some medications used to manage spasticity are also important in regulating the fusimotor drive (e.g., [9]), as are some neurotransmitters (e.g., [10]). But, how exactly do these pharmacological imbalances or re-balances lead to functional changes?

We took to heart Richard Feynman's idea that *'What I cannot build I do not understand'* and used the synthetic analytic approach to build a physical implementation of the closed-loop behavior of the fusimotor drive in the spinal stretch reflex response. We extended a computational neuromorphic system emulating spinal and transcortical stretch reflex loops [11], and created a hardware-in-the-loop neuro-mechanomorphic system capable of controlling robotic and cadaveric fingers in the physical world as discussed in Part I of our work [12]. In this work — Part II — we present a systematic application of this neuro-mechano-morphic system to explore the effect of different combinations of fusimotor drive on the nuances of the reflex force response. To do so, we replicated the classical neurophysiological paradigm to elicit stretch-reflexes via ramp-and-hold perturbations of human fingers (see Methods).

$\LaTeX\, 2_\varepsilon$     3

## 2. METHODS

### 2.1. Neuro-mechano-morphic System

The Neuro-mechano-morphic system shown in Figure 2 was used for the experiments. This setup has been equipped with state-of-the-art models of populations of muscle spindle and their $\gamma$-motoneuronal drive along with populations of $\alpha$ motor neurons and their recruitment and rate coding properties, in addition to a mathematical muscle model — all running in real-time [11, 13]. The aforementioned mathematical models emulate the final muscle forces and interact with a mechanical plant in real-time, consisting of a joint - either robotic or cadaveric, tendons and electrical motors ‡. In Part I of this work, we demonstrate this methodology by successful integration of the model emulator with a mechanical plant (robotic or cadaveric joint) in real-time [12]. We now present a systematic exploration of the effects of different levels of fusimotor and cortical drive.

*2.1.1. Cadaveric Preparation:* To include the actual tendon compliance and corresponding moment arms, as in our prior work [14, 15], we resected a fresh frozen cadaver arm at the midforearm level which was dissected the proximal end of the insertion tendons of the *Flexor Digitorum Profundus* (FDP) and *Extensor Indicis Proprius* (EIP) muscles of the arm. The proximal ends of these tendons were tied and glued to two high tensile strength para-aramid strings (Kevlar Model 8800K43). Additionally, the wrist was rigidly mounted to the experimental table using an external fixator (Agee WristJack, Hand Biomechanics Lab, Inc., Sacramento, CA). The movements of the proximal and distal interphalangeal joints were also arrested using finger splints.

*2.1.2. Control Loops:* Figure 3 shows the schematic of the real-time control loops. The first is the spinal and transcortical reflex loop which provided the tendon reflex force. The FPGAs function as controllers and plant was the *metacarpophalangeal* (MCP) joint of the cadaveric index finger. Part 1 of this work details the mathematical models implemented in the controller. The strings that were fastened to the tendons were connected to DC motors (Faulhaber 3863H024C). The motor driver featured an array of Western Design LDU-S1 high-current Darlington drivers running on the PCU-S3 Chassis. The rotational movements of the motors were recorded using shaft encoders

‡ A point of clarification: We use the term emulation as distinct from simulation and control. In our point of view, emulation is the realistic implementation of the mechanisms of interest, running at the same time-scale as the biological system being studied. By contrast, simulation includes generic black-box implementations that provide realistic input-output relations but need not implement the mechanisms of interest in real-time nor be coupled to the real mechanics of the system. Further, the goal in control theory is to achieve a certain criterion, e.g. stabilizing the system, minimizing the error between desired and measured signals, etc. The approach expounded in this work does not explicitly control the stability or simulate the input-output characteristics of the joint. Rather, the system allows the emergence of behaviors that are analogous to those exhibited by biological systems

$\LaTeX\,2_\varepsilon$ 4

(HEDS-5500). A custom computer application calculated the musculotendon lengths from the encoder pulse train and provided them to the FPGA.

The second control loop regulated the tendon forces to closely follow the reference forces provided by the FPGA. Thus, a *Proportional-Integral* (PI) controller, programmed into the app controlled the output forces of the tendons. Load cells (Interface model SML-10) measured the tendon forces and their outputs were amplified and low-pass filtered using a signal conditioning module (Transducer Techniques TM0-1-12 VDC).

A DC Servo motor (Dynammixel RX-28), whose axis of rotation was aligned to that of the MCP joint, delivered position perturbations to the joint. The servo was programmed to be much stiffer than the finger joint and the muscle (tendon) force responses did not significantly change the position of the servo and hence did not stretch the antagonist muscle. Consequently, the two muscles could be analyzed independently.

*2.1.3. Neuromorphic System:*    Briefly, as described in Part I of our study as well as [16], a set of three FPGAs (OpalKelly XEM6010-LX150) emulated the stretch reflex loops for each muscle (total six FPGAs for the antagonist muscle pair). The *sensory* FPGA was fed with the static ($\gamma_s$) and dynamic ($\gamma_d$) fusimotor drives (set by user) and the measured muscle length to emulate an ensemble of 128 muscle spindles (Figure. 1) with primary (Ia) and secondary (II) afferents. We used the model developed by Mileusnic et al. which showed a close fit to the afferent firing rates recorded experimentally in a range of different experimental conditions [17]. This model incorporates the three nonlinear intrafusal fibers (viz. bag$_1$, bag$_2$, and chain fibers) that contribute to the firing rates of primary and secondary afferents. The model features realistic temporal properties of fusimotor activation as well as partial occlusion.

The primary and secondary afferents of the ensemble of muscle spindles made synaptic connections with the motor neuron pool in the *motor* FPGA via a monosynaptic pathway with a delay of 32ms representing a simplified model of the short latency component of the stretch reflex loop. The spinal projection from secondary afferents to alpha motor neurons in the model reflects various interneuronal pathways rather than a monosynaptic loop, which has not been described [1]. Both the primary and secondary afferents also made synaptic connections to the same motor neuron pool via the *cortical* FPGA with a delay of 64 ms and represents a very simplified model of the long latency, transcortical component of the stretch reflex loop circuitry. The cortical FPGA emulated 128 neurons which is a clear oversimplification of the real biology. The cortical neurons had a user-defined tonic drive which functioned as a descending cortical offset to the motor neuron pool. The motor FPGA emulated models of motor neuron pool (with recruitment and rate coding) and a skeletal muscle while delivering the muscle force, EMG and motor neuron pool raster to the real-time custom computer program over *USB 2.0* buses. The total number of neurons emulated for each afferented muscle was 1152 (total 2304 for the antagonistic muscle pair) which consisted of 256 spindle afferents (primary and secondary), 128 cortical neurons and 768 motor neurons.

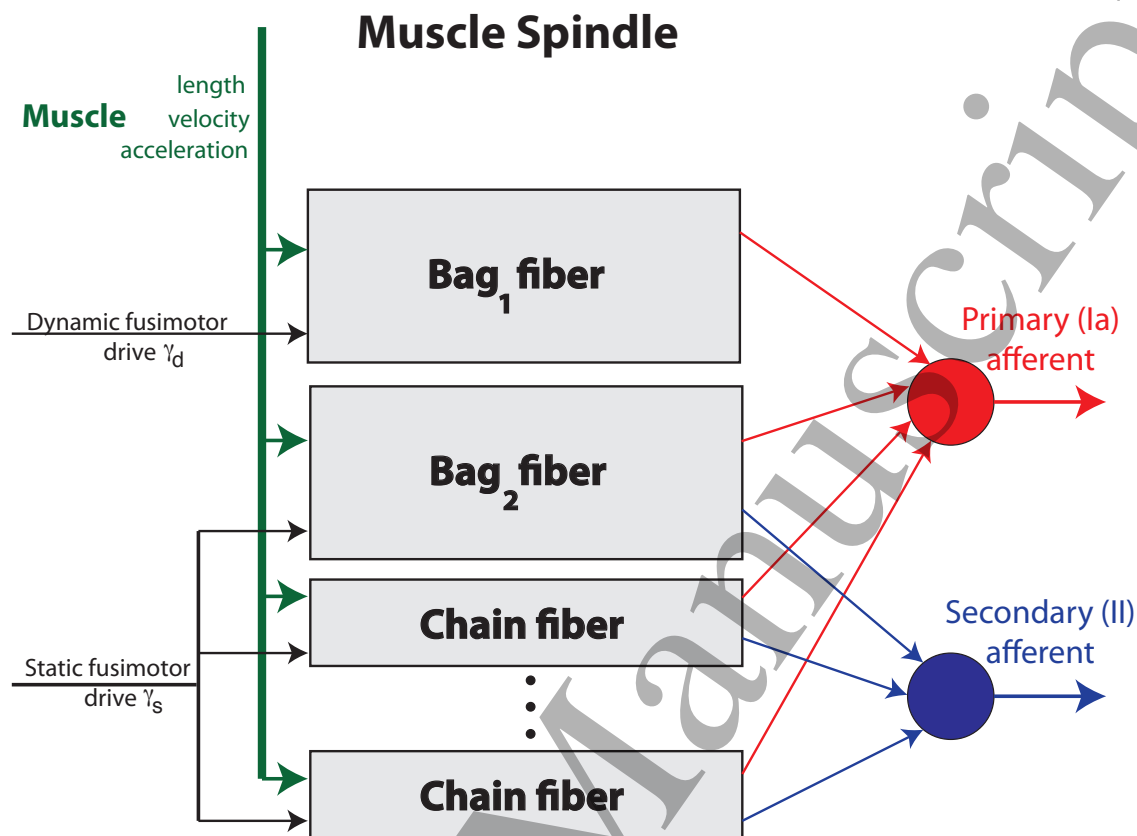$\mathit{L\!A\!T\!E\!X}\,2_\varepsilon$                                                                 5



**Figure 1.** A typical muscle spindle consists of a capsule incorporating one bag$_1$, one bag$_2$ and 5-10 chain intrafusal muscle fibers with helical sensory transduction zones from one primary afferent on all intrafusal fibers and from two secondary afferents ending on only the bag$_2$ and chain fibers. Static fusimotor neurons evoke contractions of the polar regions of the bag$_2$ and chain fibers, stretching transduction zones of all afferents. Dynamic fusimotor neurons cause a viscous stiffening of the polar regions of the bag$_1$ fiber, increasing the sensitivity of the primary afferent to velocity of stretch [17].

The FPGAs simulated the models at a sampling rate of *1 KHz*.

*2.2. Data Acquisition*

All data acquisition was performed using a high-performance National Instruments (NI) *PXI-8108* real-time computer, upgraded with 4 GB DDR2 RAM and a 500 GB SSD. An NI *PXI-6254* ADC card recorded the muscle forces while muscle lengths were recorded using a NI *PXI-6602* digital I/O card. The force trajectory generated by the PI controller was input to the motor driver via a NI *PXI-6723* DAC card. All of the data acquisition hardware was housed in the NI *PXI-1042* chassis.
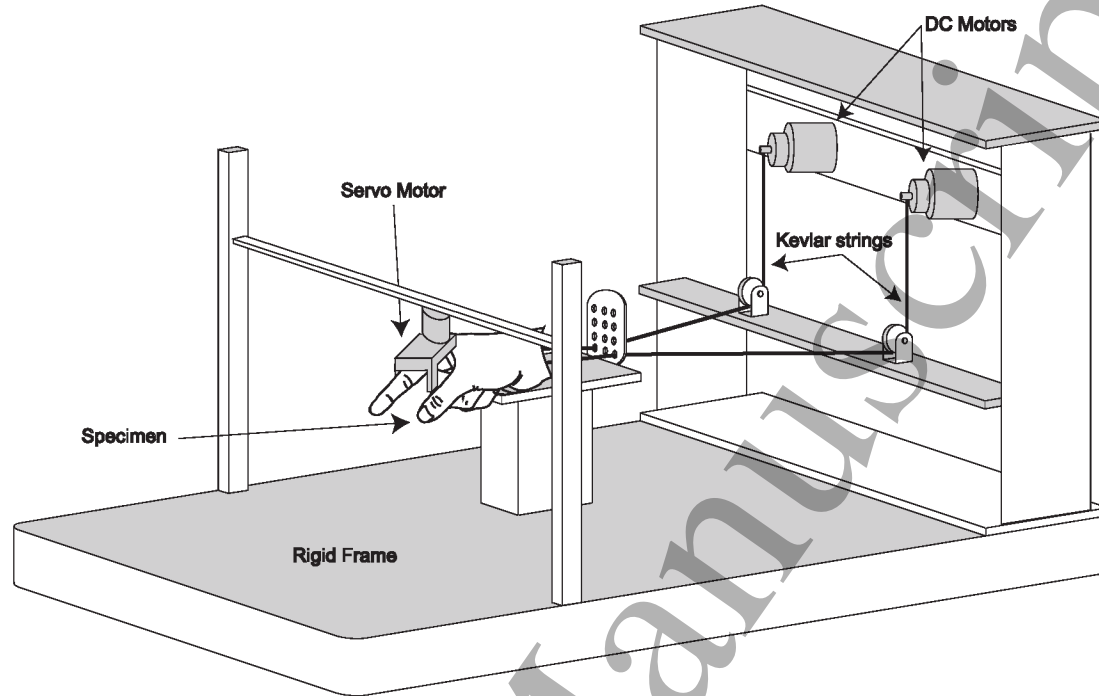
**Figure 2.** Schematic of the neuromechanomorphic system, our experimental setup. A servo motor applied ramp-and-hold perturbations to the MCP joint of the cadaveric hand mounted rigidly on the experimental table. Tendon lengths and changes in tendon lengths due to the perturbations were recorded and provided to a set of FPGAs in real-time. The FPGAs were running in real-time, emulating the stretch reflex loops and provided the tendon force trajectories. Finally, DC motors actuated the tendon forces to follow the reference force trajectory.



**Figure 3.** The neuromechanomorphic design consists of two feedback loops: ($i$) the spinal and transcortical reflex loops running on FPGA, emulating the stretch reflex mechanism; ($ii$) the force controller loop, running on C++ to regulate the force output.

$\mathrm{\LaTeX\,2}_\varepsilon$ 7



**Figure 4.** Flowchart of the C++ code interfacing the neuromorphic system with the anatomical plant. It is a multithreaded program: FPGA thread read and write signals from and to the sensory and motor FPGAs; the controller thread is a real-time thread for communication t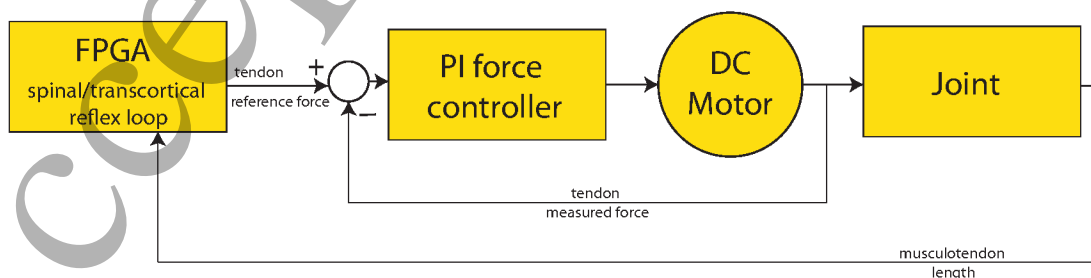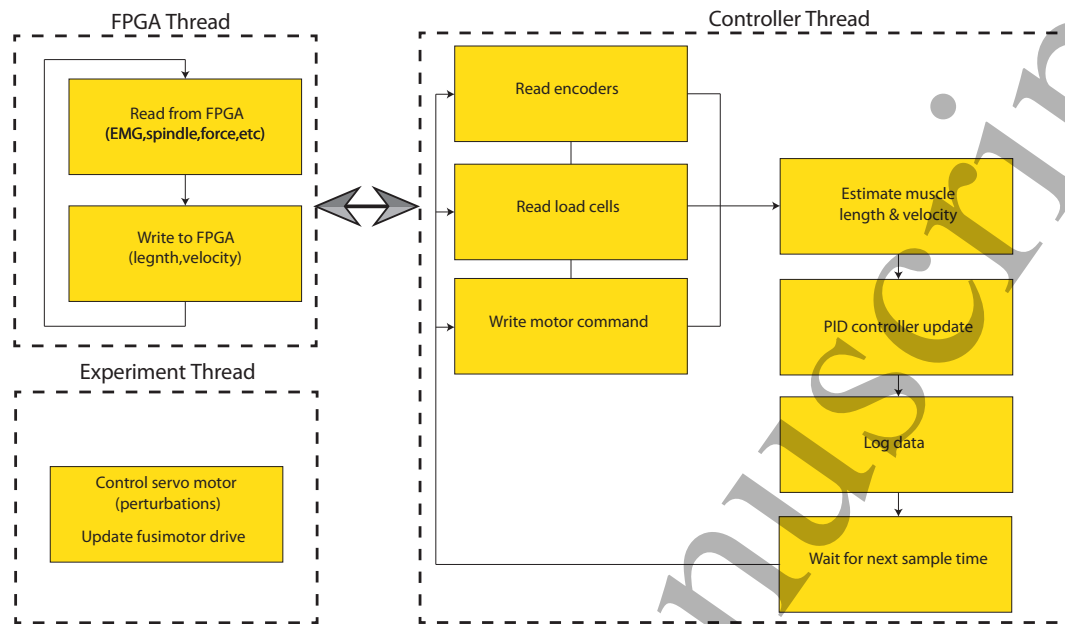o the ADC and DAC cards, implementing the force control PID controller and logging data; the experimental thread is a state machine running the experiments and updating the state of the servo motor perturbing the joint.

## 2.3. Host Program

Figure 4 shows the flowchart of the host computer application programmed using C/C++, featuring multithreading with three concurrent, low-latency threads. The thread handling FPGA communications interacts with the sensory and motor FPGAs, transmitting muscle length and velocity to the FPGAs while receiving muscle emulated force, EMG and spindle Ia, II signals from them. The emulated force that was just received now acts as the reference force for the PI controller which operated in another independent thread. This controller thread is accurately regulated to update every 1 millisecond and controls time sensitive tasks. It is the core of the *real-time* program since it enforces the sampling rate on the system and communicates with the ADC/DAC cards at each sample time and updates the values for muscle length and velocity, while implementing the PID force controller. The third thread is a state machine controlling the experiment, updating the fusimotor drive, voluntary cortical drive and controlling the servo motor applying the joint perturbations.

## 2.4. Systematic Exploration of The Reflex Response Parameters

We perturbed the MCP joint using conventional ramp-and-hold perturbations similar to those employed previously published experiments with human subjects [18–20]. The

$\mathcal{B}T_{E}X\,2_{\varepsilon}$ 8

firing rates of the static ($\gamma_s$) and dynamic ($\gamma_d$) fusimotor neurons were independently selected from the set $\{0, 25, 50, \cdots, 200\}$ which were all in the range of values validated in previous work for our spindle model [17]. By selecting values from this grid at random, it was possible to mitigate the potential confound of presentation order given that tissue response, such as tendon stiffness, can change over time as the collagen fibers may reorganize themselves in response to load. We also randomly varied the velocity of perturbations among the four values $\{50, 100, 200, 300\}$ (degrees/s) and the three baseline cortical drive ($c$) among the three values of $\{0, 5, 10\}\%$ MVC by changing the baseline firing rate of the cortical neurons. We randomly selected combinations of parameters exhaustively, with each combination being tested only once. With four perturbations for each combination, the experiment constituted $9 \times 9 \times 4 \times 3 \times 4 = 3888$ ramp-and-hold perturbations.

### 2.5. Analysis

Given that the stretch reflex loop is sensitive to both the muscle length and velocity, we analyzed the responses for both the phasic and tonic intervals of stretch [21]. We segmented the responses per [22, 23]: ($i$) the phasic interval was 1400 (ms) starting at the onset of the perturbation; ($ii$) the tonic interval was 450 (ms) following the phasic interval. Figure 5 demonstrates how we defined the tonic force response as the difference between the baseline and the average of the response in the tonic interval. We further defined the phasic force response as the difference between the peak of the response during the phasic interval and the average tonic reflex amplitude. We then computed these measures across all combination of parameters.

## 3. RESULTS

Figure 5 demonstrates typical emulated (i.e., commanded) and actual (i.e., measured) closed-loop force responses to a rotational perturbation that induces lengthening of muscle fibers. Both force responses (Figure 5(B)) consist of a transient (phasic) and a steady-state (tonic) response. These emulated closed-loop force responses contain instantaneous contributions from the force-length and force-velocity properties of the muscle and the delayed reflex responses themselves. For consistency in the instantaneous responses, we set all ramp-and-hold perturbations to start at the joint flexion angle of 24 (degrees) and end at the joint extension angle of 18 (degrees). This way, all the changes that we see in our reflex responses are mostly due to changes in fusimotor and cortical drives as would be the case in living muscle. The principal differences between the emulated (Figure 5(B)) and measured forces (Figure 5(C)) arise from the nature and implementation of our muscles model, the bandwidth of the control loop of the brushless DC motors, plus the inertial and viscoelastic properties of the motors and tendons. These properties of the engineered and anatomical components led to high-frequency ringing and some delay in the ramp-up and ramp-down phases of the measured

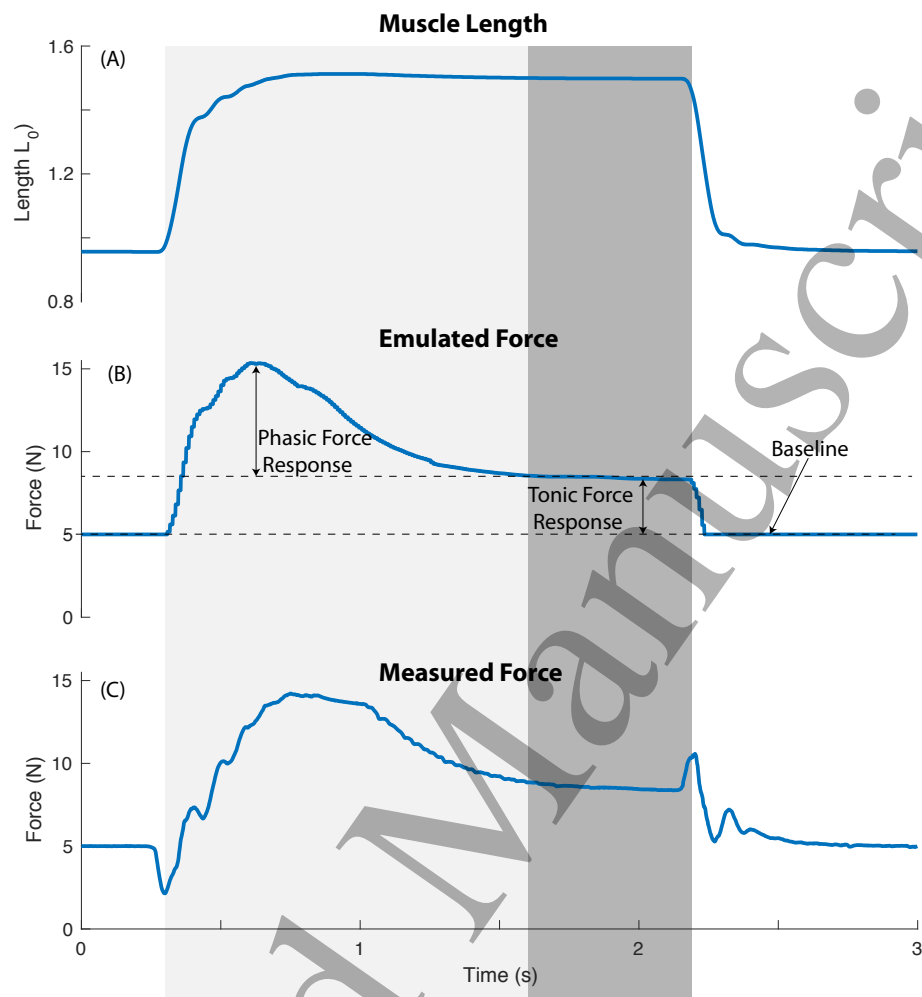$\mathit{L\!AT\!E\!X}\,2_\varepsilon$                                                                                                9



**Figure 5.** Typical force response to ramp-and-hold perturbation with velocity of 300 (degrees/s) is segmented to phasic and tonic intervals. We computed the reflex phasic and tonic amplitudes as illustrated in the figure. The phasic interval was 1400 (ms) long starting at the onset of the perturbation. The tonic interval was 450 (ms) long following the phasic interval: (A) muscle length; (B) muscle emulated force; (C) measured force in the cadaveric tendon.

force responses. These force fluctuations are similar to those reported during length perturbations in human muscles [23, 24]. Thus, these differences between emulated and measured force responses do not challenge the validity of our results. These fluctuations might in turn result in small changes in the muscle fascicle length and consequently spindle length, inducing fluctuations in the afferent firing rates during these ramp phases as evident in Figure 6.

Figure 6 shows representative responses to the ramp-and-hold perturbation at four different levels of fusimotor and cortical drives. First and foremost, we note that the primary characteristics of the responses were qualitatively similar to experimental observations [18, 20, 25]. The afferent firing rates rapidly peaked at the onset of the phasic interval and then decayed to a steady-state shortly thereafter. This resulted in

$\LaTeX\, 2_\varepsilon$                                                                                                        10

large bursts of response in the EMG during the ramp with mostly background activity during the hold. Similarly, both emulated and measured force responses peaked at the ramp interval and reached a steady-state at the hold interval.

Inspection of the representative responses reveals that the fusimotor and cortical drives significantly modulated responses at all levels of the system. A 200 (pps) increase in $\gamma_d$, predictably, increased the firing rate of the primary (Ia) afferent during the ramp up from 500 to 810 (pps), but had only a small effect on the response of the secondary (II) afferent (increase of 10 (pps)). As a result, the ramps led to rapid recruitment of additional motor units — which in turn led to rapidly increased EMG and force (Figure 6 column 1 vs column 2). Thus, an increase in $\gamma_d$ increased the phasic force response.

Conversely, increasing the $\gamma_s$, and $c$ (i.e., static fusimotor and cortical drives), increased the responses during the hold (Figure 6 column 1 vs columns 3-4). Increasing $\gamma_s$ by 200 (pps) also clamped offsets to the firing rates of both the primary (increase of 122 (pps)) and secondary (increase of 56 (pps)) afferents. Moreover, increasing the $\gamma_s$, and $c$ also have the expected effect of increasing the baseline $\alpha$ motor neuron activity. This is seen clearly in columns 3-4 as increased $\alpha$ motor neuron activity before and after the muscle is lengthened.

Figure 7(A-B) illustrates the phasic and tonic force responses averaged across all four ramp velocities as a function over the 81 combinations of $\gamma_s$ and $\gamma_d$ with zero cortical drive. We present the average across all ramp velocities for the sake of brevity because we saw the patterns was consistent across them. The contour plot for the phasic force response (panel A) shows concentric arcs illustrating both (i) the direct relation of the phasic amplitude to the dynamic fusimotor drive and (ii) its inverse proportionality to the static fusimotor drive. In contrast, while there was no strong correlation of tonic force response with dynamic fusimotor drive (panel B), the more vertical pattern suggests that force responses increased monotonically with static fusimotor drive.

Figure 7(panels C-F) show the contour plots for responses with active cortical drive. Visual inspection of the phasic force response (panels C and E) reveals a similar response as for zero cortical drive (panels A), but illustrates a decrease in overall amplitude with an increase in cortical drive. In contrast, there was a sharp increases in the overall tonic force response in the presence of cortical drive (note light color of panels D and F). Note, however, that even when the sensitivity to fusimotor drive decreased with cortical drive (panel D and F), we see an island of lower force response that suggests a nonlinear, or at least non-monotonic, dependence on $\gamma_s$ and $\gamma_d$ (panel F).

So far, we have found that $\gamma_d$ mostly modulated the phasic force response while $\gamma_s$ modulated both the phasic and tonic amplitudes. Moreover, the sensitivity of these relationships could be altered by modulating the cortical drive. To quantify these effects, we calculated the slope of the linear regression on all 9 vertical slices from the phasic responses in Figure 7(panels A, C and E). Figure 8 (A) shows that the sensitivity (i.e., slope) of the phasic force response to $\gamma_d$ decreased as a function of $\gamma_s$. Changing the cortical drive affect the values slightly, but not their trend.
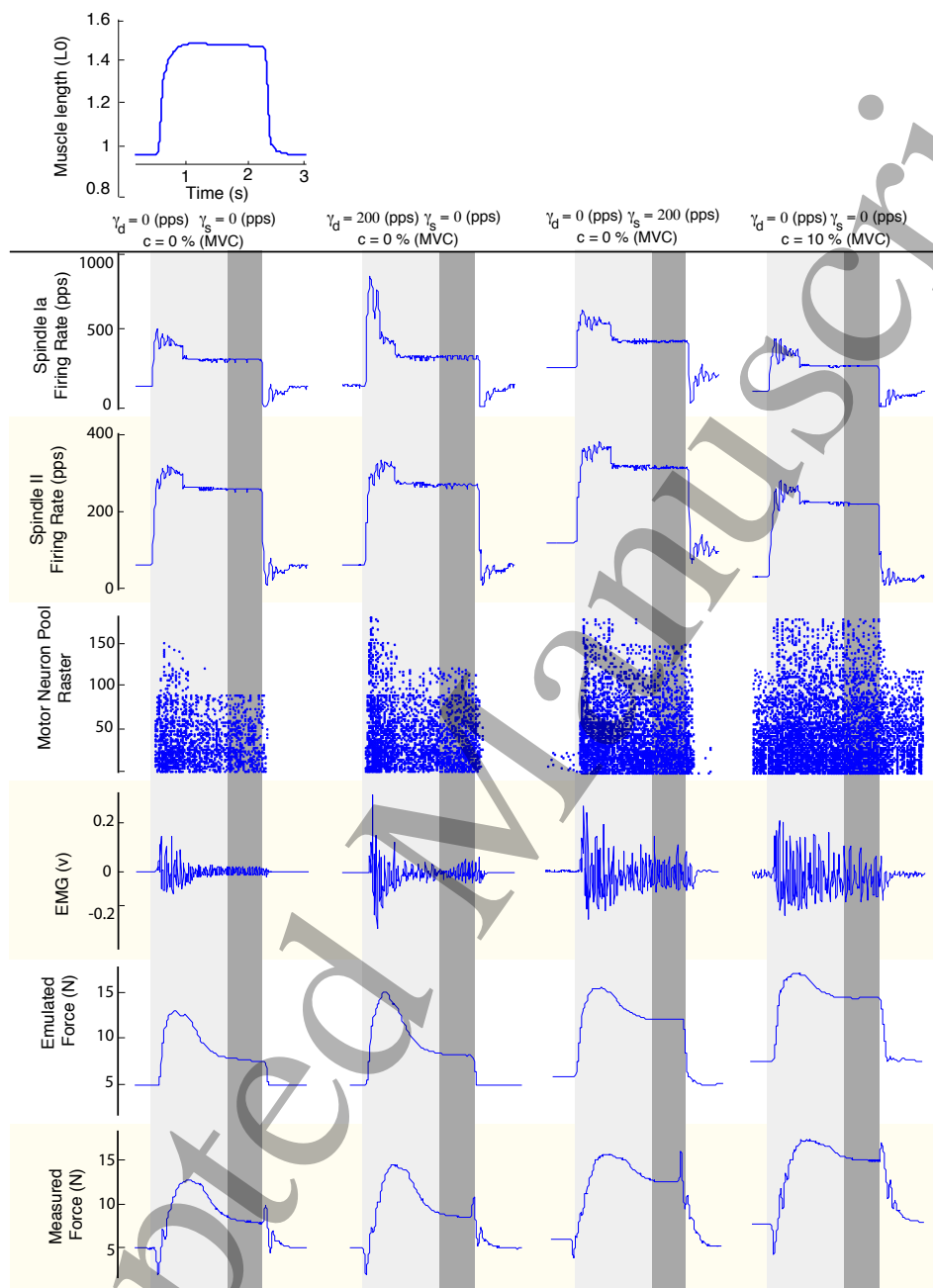
**Figure 6.** Representative responses of spindle Ia (first row), spindle II (second row), motor neuron pool raster of 192 motor units from the smallest (1) to the largest (192) unit (third row), EMG (fourth row), emulated force (fifth row), measured force (sixth row) to ramp-and-hold perturbation with velocity of 300 (degrees/s) with different fusimotor and cortical drives: dynamic ($\gamma_d$) and static ($\gamma_s$) fusimotor and cortical ($c$) drives are zero (first column); dynamic fusimotor firing rate is 200 pps and cortical and static drives are zero (second column); static fusimotor firing rate is 200 pps and cortical and dynamic drives are zero (third column); both static and dynamic fusimotor drives are zero and cortical drive is 10% (MVC) (fourth column).

$\mathcal{L\!AT\!E\!X}\,2_\varepsilon$

12



**Figure 7.** Contour plot of the mean value of the phasic and tonic force response as functions of the static and dynamic fusimotor firing rates averaged across all four ramp velocities: (A,B) phasic 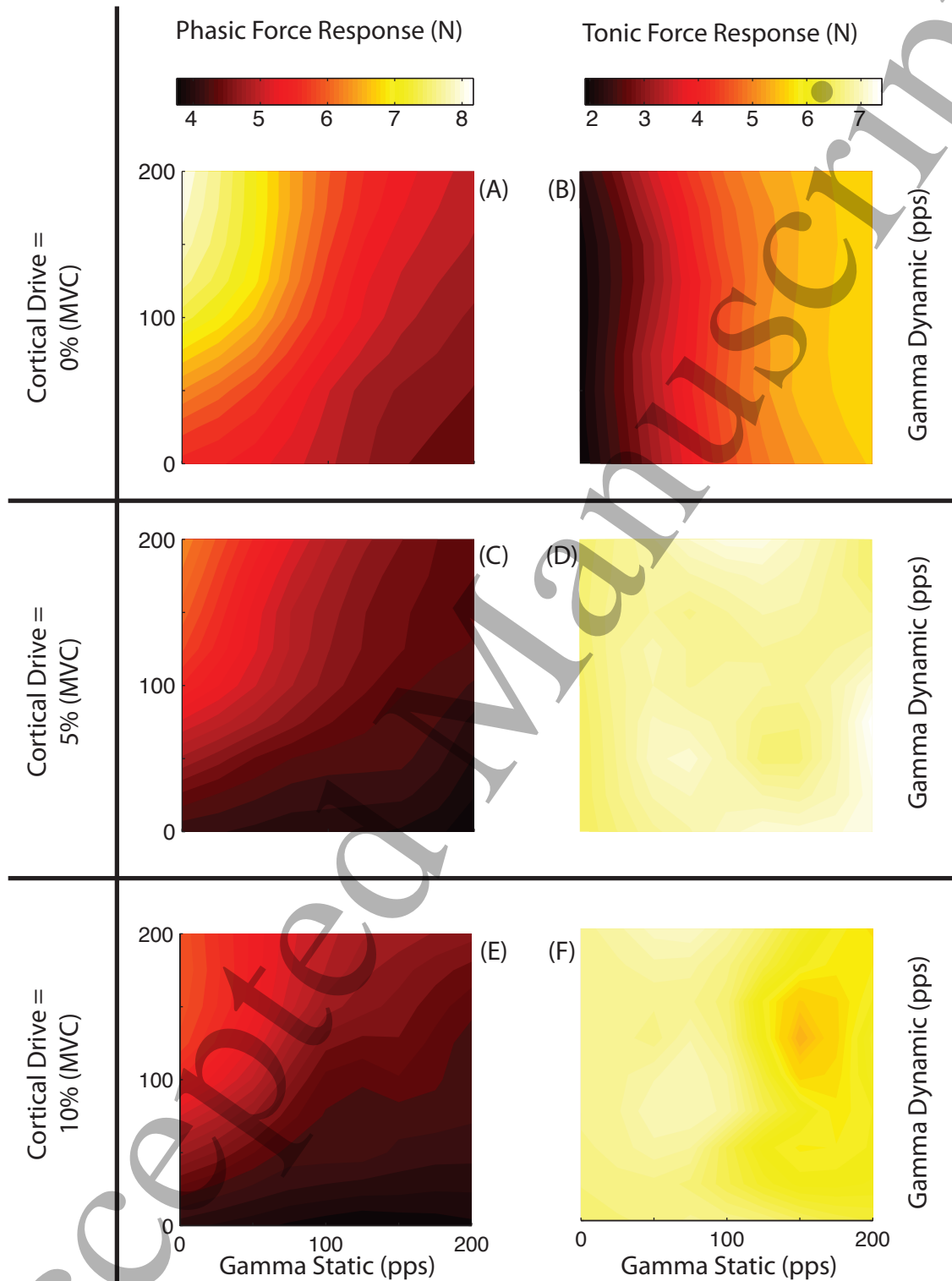and tonic force responses at cortical drive of 0 % (MVC); (C,D) phasic and tonic force responses at cortical drive of 5 % (MVC); (E,F) phasic and tonic force responses at cortical drive of 10 % (MVC).

$\mathit{L\!A\!T\!E\!X}\,2_\varepsilon$                                                                13
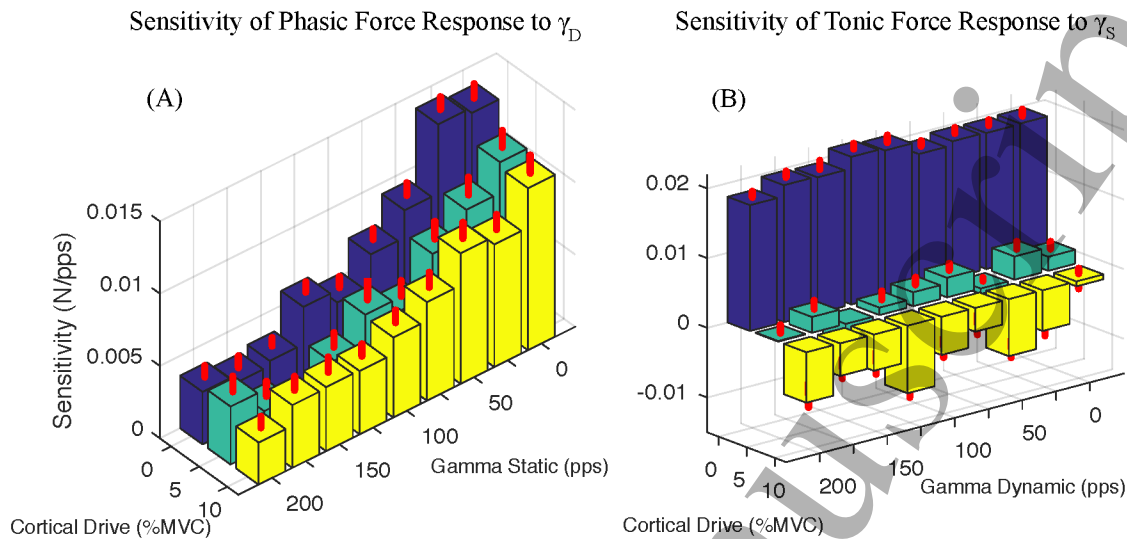


**Figure 8.** Sensitivity of the reflex amplitudes to the fusimotor drives change as functions of fusimotor and cortical drives (mean and standard deviation averaged across all four ramp velocities). Sensitivity was defined as the derivative of the phasic and tonic force responses as a function of the static and dynamic fusimotor drives. (A) Sensitivity of the phasic force response to the dynamic fusimotor drive as functions of static fusimotor and cortical drives; (B) sensitivity of the tonic force response to the static fusimotor drive as functions of dynamic fusimotor and cortical drives.

We similarly quantified the sensitivity of the tonic force responses to $\gamma_s$ using the same linear regression approach, but now applied to horizontal slices of Figure 7(panels B, D and F). Figure 8 (B) demonstrates sensitivity of the tonic force response to $\gamma_s$, which did not change with $\gamma_d$. However, for non-zero cortical drive there was no sensitivity to either static or dynamic fusimotor drive.

Previous experimental studies have revealed that variability of muscle force is proportional to the mean force exerted, i.e. signal dependent noise [26, 27]. This gave us the opportunity to run a simple experiment where, in a set of isometric contractions, we systematically increased the cortical drive to the muscle from 0 to 100% (MVC) in steps of 3.3% (MVC). This resulted in 30 trials, each lasting 10 s. We computed the average and standard deviation of force for each trial. Figure 9 demonstrates that the standard deviation of force increases linearly as a function of its average similar to the experimental observations in isometric force production experiments. Consequently, an important emergent property of our setup is in that signal dependent motor noise emerges naturally even though it was not explicitly built into our model. The linear scaling of force variability as a function of the mean force level in our system is presumably as a result of the Hennemans size principle built into our motor neuron pool. This mechanism has been proposed by Jones et al. as a source for signal dependent noise [28].
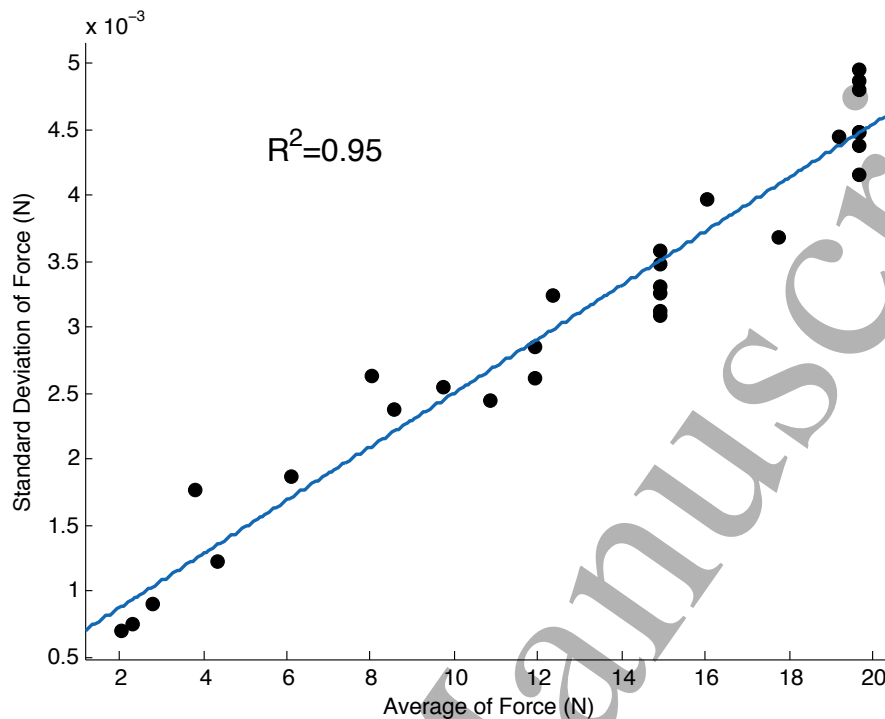
$\LaTeX\, 2_\varepsilon$     14



**Figure 9.** Signal dependent noise, an emergent property of our system. Variability of the force in isometric force generation tasks increases as a function of the average of the force.

## 4. DISCUSSION

### 4.1. Closed-Loop Effect of Fusimotor Drive on the Stretch Reflex Response:

We studied the fundamentals of muscle afferentation by building a real-time neuro-mechano-morphic system. We find that this physiologically faithful implementation of the spinal and transcortical stretch reflex circuitry produces stable and robust *closed-loop* responses to ramp-and-hold perturbations for a wide range of levels of $\gamma_s$ and $\gamma_d$ fusimotor drives. We found that $\gamma_d$ mostly modulated the responses of the primary Ia afferents, EMG and force during the phasic interval (i.e., ramp). In contrast, $\gamma_s$ modulated responses at all levels during the hold interval. To our knowledge, this is the first exhaustive exploration of the robustness of the closed-loop monosynaptic spinal and transcortical stretch reflexes.

As one would expect, several nontrivial behaviors arose from coupling our neuromorphic circuits with anatomical tendons and joint structures. Chief among these is the nonlinearity in response across fusimotor parameter values and cortical $\alpha$-motoneuron drive, the complex force responses within a given ramp-and-hold perturbation, and the effects of tendon viscoelasticity. Our study reveals challenges not previously recognized in the motor control literature about the neural control of even simple stretch reflexes during interaction with compliant tendons and physical

LaTeX $2_\varepsilon$                                                                                 15

environments. These challenges are then amplified when we consider that the nervous system must control and coordinate the effects of such parameter changes across multiple muscles — and over time during everyday tasks. Interestingly, we saw that the changes with fusimotor parameter values were consistent across ramp velocities (Figure 7). This is not necessarily unexpected because changes in ramp velocity simply induce a monotonic change in spindle output. However, this work enables a future systematic exploration of the effect of ramp velocity (e.g., [19]) on reflex responses — as done in clinics — to understand the role of fusimotor drive on healthy tone and pathologic catch responses.

As has been previously documented in many experimental studies, the CNS is capable of adjusting the sensitivity of the stretch reflex loop [29]. In particular, the sensitivity of the phasic force response to $\gamma_d$ decreased with an increase in $\gamma_s$ (Figure 8 (A)). This was presumably due to the partial occlusion mechanism modeled into our muscle spindle. We also observed that the sensitivity slightly decreased with increase in the cortical drive. Exploring the muscle length data revealed that the baseline of muscle length was 2.9% shorter and the muscle stretch to ramp-and-hold perturbation of the joint was 1.9% shorter with background cortical drive. This is likely due to the elastic nature of the real tendons that stretched under baseline cortical drive and decreased the muscle length, as well as phasic and tonic tensions. This resulted in shorter muscle fibers. Afferent firing rate is lower when the muscle is shorter, and this decreased the phasic force response. Decrease in the phasic force response with increase in tonic contraction level in normal human has been previously reported in the literature but had remained difficult to explain [22, 30].

The sensitivity of the tonic force response to $\gamma_s$ did not change with increase in $\gamma_d$ (Figure 8(B)). This was because $\gamma_d$ is increasing the firing rate of primary Ia afferents only at the ramp interval, increasing only the phasic force response. However, the sensitivity of the tonic force response to $\gamma_s$ decreased dramatically with increase in cortical drive. But, what are the underlying mechanisms responsible for this? The 2.8% reduction in muscle length because of strain in the tendons cannot be the only mechanism. We carefully inspected the spindle and motor neuron rasters as illustrated in Figure 10. It is evident that the static fusimotor drive increased the secondary firing rate with and without cortical drive (Figure 10(A) all columns). However, the tonic force response sensitivity to $\gamma_s$ was sensitive to this increase when cortical drive was zero (Figure 10(C) column 1 and 2) but not sensitive at all when cortical drive was active (Figure 10(C) column 3 and 4). Motor neuron raster demonstrates that $\gamma_s$ alone could not significantly increase the force baseline (when the muscle was shortened) with no cortical drive (Figure 10(B) column 1 and 2). This was because the motor neuron pool was not active and thus motor units were far from their thresholds. However, $\gamma_s$ significantly increased the baseline when cortical drive was active (Figure 10(B) column 3 and 4). This was mainly because the cortical drive recruited the smaller motor neurons and thus facilitated the recruitment of larger ones with $\gamma_s$. Since the baseline increases in parallel to tonic force with $\gamma_s$, it only shifts the offset of the force and is unable to

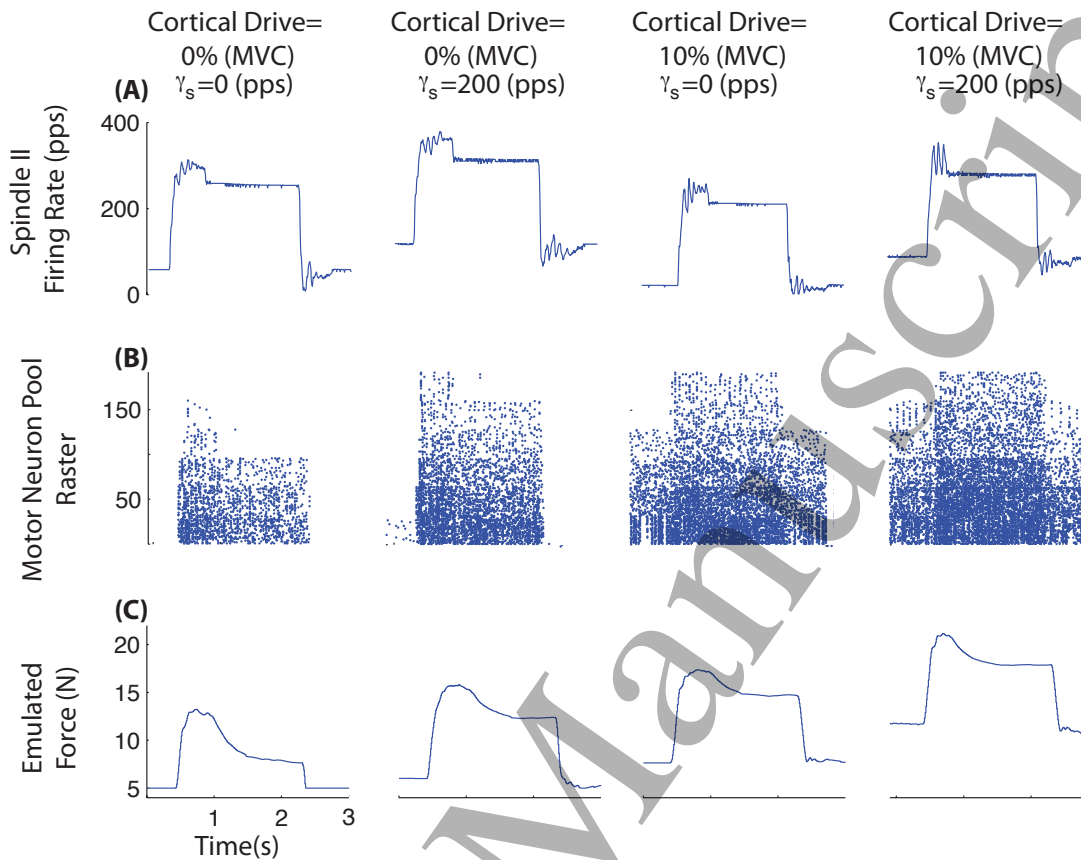$\mathcal{L\!A\!T\!E\!X}\,2_\varepsilon$                                                                            16



**Figure 10.** Sensitivity of tonic force response to $\gamma_s$ decreases when there is background voluntary activity: (A) firing rate of spindle secondary afferent (the most sensitive afferent to $\gamma_s$) increases with $\gamma_s$; moreover, the firing rate of spindle is slightly decreased with voluntary, background activity which is due to the shorter muscle length when the muscle is voluntarily contracting; (B) motorneuron rasters show that the firing baseline (in the shortening phase of the perturbations) is absent or very small when the voluntary drive is absent and increases significantly with the voluntary drive, recruiting the smaller motor units; (C) muscle force shows that tonic force response increases with $\gamma_s$ when voluntary drive is absent. The reflex tonic force is less sensitive $\gamma_s$ in the presence of voluntary drive because both the force baseline and the absolute value of the force in the hold interval increase with $\gamma_s$.

increase the tonic force response and thus the response becomes insensitive to $\gamma_s$.

One can argue the the large scale trends in reflex response seen in our color maps (Figure 7) are to be expected and make sense. However, it is important to note that these properties emerged from interactions among elements that to our knowledge had not been connected previously. Moreover, it is equally interesting to note that the departure from linear trends must pose challenges to the nervous system when controlling afferented muscles. These difficulties are further exacerbated when, as in the case of tonic response with 10% cortical drive, the response is not monotonic across the parameter space. This can be seen as islands of high and low activity within the

$\mathcal{L\!A\!T\!E\!X\,2_\varepsilon}$                                                                                                17

colormap. These nonlinearities (or at times departure from monotonicity) likely come
about in part from the nonlinear nature of the spindle model [17] — which to our
knowledge is the most physiologically faithful model in the literature.

### 4.2. Why Neuromechanomorphic Emulation?

This work extends the work of Sreenivasa et al [31] by using a synthetic neuro-mechano-
morphic system to emulate the stretch reflex loop because our FPGA system can emulate
the populations of neurons and control the mechatronic system in true real-time while
emulating the physiological delays and neuromechanic multi-scale interactions. It is
even capable of operation in hyper-time (365x real-time) to predict long-term changes
of sensorimotor function [13]. This allowed us to use the MCP joint of a cadaveric hand
as the plant to ensure anatomical and physical fidelity. This enables us to perform
realistic simulations and confront the very challenge the central nervous system faces
when actuating actual tendons crossing anatomical joints [14, 15, 32]. A number of
desirable features include: realistic viscoelastic properties of the joint, passive tissues and
tendons, and realistic strain in loaded tendons and their non-constant moment arms [33].
These will result in realistic muscle lengths changes due to external perturbations that
are quite difficult, if not impossible, to model and implement faithfully in computer
simulations [34].

Therefore, this system is not simply doomed to succeed, but represents what is
to our knowledge the first real-world implementation of the fundamental mechanisms
and features of the stretch reflexes when coupled to real anatomical systems. The
real power of this system is to provide a substrate on which to add the complexity
as required to account for able motor function and pathology. Future work will be
able to disambiguate whether and how the response of the system is due to neural or
anatomical elements by systematically comparing this baseline behavior to that arising
when individual elements are replaced by alternative implementations (e.g., changing
muscle models, varying the degree of randomness in the spiking of individual neurons,
changing the synaptic weightings, using inextensible tendons or tendons with varying
degree of elasticity, constant moment arms, etc). Similarly, we will add other known
elements such as Golgi tendon organs, Renshaw cells, Ib interneurons, etc. to understand
their contributions above and beyond the behavior of this basic reflex circuitry.

### 4.3. Emergent Properties:

It is important to note that because of lack of objective models and limited computation
power, it would be difficult, if not impossible to replicate all behaviors of the
neuromuscular system. However, in a reasonable model, these behaviors should emerge
naturally as a result of interaction among fundamental components of the system. Here
we have observed and documented some of these emergent properties. Examples include
phasic and tonic reflex responses to a ramp-and-hold perturbation, and signal dependent
noise as shown in this paper; as well as maintaining a stable posture following a transient

$\mathcal{L\!\!AT\!\!E\!X\,2_\varepsilon}$                                                                                        18

force perturbation to the joint as shown in the companion paper [12]. In future, we will explore other emergent properties of the system (see scientific and clinical implications below).

### 4.4. Limitations of the Study:

Numerical simulations are promising tools to understand healthy function, disease and role of therapeutic intervention [34]. In the context of afferented muscles [17,35], several different mechanisms can potentially contribute to pathological muscle tone such as fusimotor drive of the muscle spindle, long-latency reflex response, inward currents, presynaptic modulation of the spindle Ia-motorneuron, interneuronal modulation of the spindle II-motorneuron projections, biasing of the various motor units with respect to their threshold and frequency-modulation nonlinearities, etc. [29]. In this paper, we chose to study the effect of fusimotor drive as the first step to understand the sufficient pathways involved to emulate healthy and pathologic responses. Our hardware limitation of being able to implement only 128 pairs of spindle afferents per muscle (natural muscles have many more) has the consequence that the aggregate strength of the afferent drive to the motor neuron pool is weaker than in its biological counterpart. Therefore, we added a scaling factor in the form of an offset and gain to increase firing rates to a level that was able to appropriately drive their respective motor neuron pools. This is why the firing rates for the spindle afferents in Figure 6 are higher than those seen in spindle afferents which rarely fire faster than 250pps [17,36]. However, we believe that this does not affect the validity of our results, and will not be necessary once we are able to implement thousands of spindle afferents.

While a model of the glutamatergic ribbon synapse from a hair cell in the cochlea was used in our work [37], there is ample evidence to support the role of serotonin synapses in the modulation of spinal reflexes and in the production of rhythmic locomotion [38, 39]. This makes the inclusion of models for these synaptic neurotransmitter a logical next step.

We used a conventional model of motor neuron pool consisted of $128 \times 6 = 768$ motor units for each muscle whose parameters were adjusted according to [40] and a simple Hill-type model of skeletal muscle [41]. It is trivial that the results might depend on the properties of the motor neuron pool such as motor unit firing rate, recruitment strategy, etc. We also believe that the choice of muscle model plays a significant role in the reflex responses (see scientific implications below). In addition, our muscle model does not yet consider the aponeuroses of these muscles, which may have more significant effects for the long intrinsic muscles [42]. Future work will test whether and how different muscle models affect force responses, including tremor and other force oscillations [43].

### 4.5. Scientific Implications:

Signal dependent noise was an emerging property of our system. This opens the possibility to study other types of motor variability such as physiologic and pathologic

$\mathit{LATEX}\,2_\varepsilon$                                                                                      19

tremor as they have been attributed to physiological mechanisms including the stretch reflex loops [44]. The system we have built is an enabling platform to study the properties of tremor and its mechanical and neural mechanisms. As such, the neural connectivity across different motor unit pools can be changed to begin to, for example, understand the nature of cortico-muscular or musculo-muscular coherence, tremor and clonus in health and disease [45, 46].

We validated the notion that the fusimotor drive can significantly modulate the stretch reflex response. But again, the main benefit of this work was to quantify the details of those responses, and how they are affected by both neural (e.g., fusimotor and cortical commands), physiological (e.g., muscle spindle structure and function), and mechanical (e.g., tendon compliance, moment arms, etc) properties. In future, it is within our goals to emulate and compare against data from pathologic responses in patients with disrupted reflexes, to find the range of fusimotor drive that is sufficient to mimic these behaviors. More specifically, we are interested to mimic spasticity and compare with clinical tests such as Modified Ashworth Scale [7, 47].

Regarding muscle function, we used a simple Hill-type muscle model with force-length and force-velocity curves that does *not* consider the dynamics of slow versus fast twitch fibers, post-activation potentiation, or dynamics of activation versus de-activation [48]. We have begun investigating other muscle models that are capable of explaining more complicated physiological phenomena as demonstrated in our companion paper [12]. By implementing a library of muscle models, our neuro-mechano-morphic setup can provide a benchmarking system to compare them in closed-loop (i.e. with muscle afferentation). This is critical in understanding the mechanisms of muscle function, for instance, the choice of muscle model in replicating nonlinear properties of joint impedance [49] or in stability of the joint in response to perturbations or in voluntary movement. Therefore, the selection of the muscle model is a known and unavoidable limitation of this work that merits further investigation by a systematic comparison for a variety of muscle models proposed in the literature — whose behavior when coupled with a closed-loop neuromorphic system remains unknown [50].

Lastly, this study reinforces the notion that the time-critical coordination of afferented muscles undergoing eccentric contractions during smooth and accurate voluntary movements remains poorly understood [51, 52], [53, 54]. Sherrington highlighted this at the birth of motor neuroscience as the problem of excitation-inhibition (refined now to include $\alpha - \gamma$ coactivation [55]) being fundamental to motor control [56]. Our recent theoretical and modeling work added details to the notion that controlling natural and compliant limb function requires careful orchestration of the obligatory changes in the lengths of all muscles in response to the rotation of a few joints—which is an overdetermined problem that is the opposite of redundant [51–53]. Our findings compound the difficulties posed by the need for appropriate $\alpha - \gamma$ coactivation by the fact that the reflex response to eccentric contractions is sensitive to multiple factors including the details of the tendon excursion and its associated departure from linearity, the physiological response of the muscle spindles, etc. This underscores the longstanding

$\mathcal{L}\!ATEX\,2_\varepsilon$                                                                                    20

difficulties in our understanding of motor control using simplified models [34, 57]. This work aims to provide a physiologically realistic platform to bring these issues to light by confronting the very challenge the central nervous system faces: using multiple afferented muscles simultaneously to pull on viscoelastic tendons that act on anatomical joints to interact with the physical world.

### 4.6. Clinical Implications:

Our goal is to understand how the musculotendon mechanics interact with spinal mechanisms to produce able and pathologic muscle function. This is significant in clinical research as a number of neuromuscular pathologies that change the muscle tone arise from presumed alterations of the spinal reflex mechanisms (e.g., changes in fusimotor drive, faulty $\alpha - \gamma$ coactivation) or compromised musculotendon structures (e.g., muscle contractures, sarcopenia, increase in motor unit innervation numbers). Even if still in the early stages of its development, our neuro-mechano-morphic system provides framework, test bed and reality check to quantify how presumed disruptions of these known mechanisms lead to pathologies, for example, in dystonia or spinal cord injury, which can be sufficiently described by simply tuning the offset and gain of the spinal or the transcortical loop [11]. Modeling other motor centers of the brain — such as the basal ganglia and the primary motor cortex — may also allow us to model hyperkinetic pathologies [58]. The system can also allow us to verify the extent to which available or proposed interventions can improve these conditions [59–61].

## 5. ACKNOWLEDGEMENT

[1] E. Pierrot-Deseilligny and D. Burke, *The circuitry of the human spinal cord: its role in motor control and movement disorders.* Cambridge University Press, 2005.

$\LaTeX\,2_\varepsilon$      21

[2] A. Prochazka, "Proprioceptive feedback and movement regulation," *Comprehensive Physiology*, 2010.

[3] G. Goodwin, M. Hulliger, and P. Matthews, "The effects of fusimotor stimulation during small amplitude stretching on the frequency-response of the primary ending of the mammalian muscle spindle.," *The Journal of physiology*, vol. 253, no. 1, p. 175, 1975.

[4] E. J. Hwang and R. Shadmehr, "Internal models of limb dynamics and the encoding of limb state," *Journal of neural engineering*, vol. 2, no. 3, p. S266, 2005.

[5] A. G. Feldman, "Once more on the equilibrium-point hypothesis ($\lambda$ model) for motor control," *Journal of motor behavior*, vol. 18, no. 1, pp. 17–54, 1986.

[6] E. Bizzi, A. Polit, and P. Morasso, "Mechanisms underlying achievement of final head position," *Journal of Neurophysiology*, vol. 39, no. 2, pp. 435–444, 1976.

[7] M. Adams and A. Hicks, "Spasticity after spinal cord injury," *Spinal cord*, vol. 43, no. 10, pp. 577–586, 2005.

[8] J. Nielsen, C. Crone, and H. Hultborn, "The spinal pathophysiology of spasticity–from a basic science point of view," *Acta Physiologica*, vol. 189, no. 2, pp. 171–180, 2007.

[9] J.-M. Gracies, P. Nance, E. Elovic, J. McGuire, and D. M. Simpson, "Traditional pharmacological treatments for spasticity part ii: General and regional treatments," *Muscle & Nerve*, vol. 20, no. S6, pp. 92–120, 1997.

[10] K. Wei, J. I. Glaser, L. Deng, C. K. Thompson, I. H. Stevenson, Q. Wang, T. G. Hornby, C. J. Heckman, and K. P. Kording, "Serotonin affects movement gain control in the spinal cord," *The Journal of Neuroscience*, vol. 34, no. 38, pp. 12690–12700, 2014.

[11] W. J. Sohn, C. M. Niu, and T. D. Sanger, "Increased long-latency reflex activity as a sufficient explanation for childhood hypertonic dystonia: a neuromorphic emulation study," *Journal of neural engineering*, vol. 12, no. 3, p. 036010, 2015.

[12] C. M. Niu, K. Jalaleddini, W. J. Sohn, J. Rocamora, T. D. Sanger, and F. J. Valero-Cuevas, "Neuromorphic meets neuromechanics part i: The methodology," *Journal of Neural Engineering*, In Review.

[13] C. M. Niu, S. K. Nandyala, and T. D. Sanger, "Emulated muscle spindle and spiking afferents validates vlsi neuromorphic hardware as a testbed for sensorimotor function and disease," *Frontiers in computational neuroscience*, vol. 8, 2014.

[14] J. L. Pearlman, S. S. Roach, and F. J. Valero-Cuevas, "The fundamental thumb-tip force vectors produced by the muscles of the thumb," *Journal of Orthopaedic Research*, vol. 22, no. 2, pp. 306–312, 2004.

[15] F. J. Valero-Cuevas, J. D. Towles, and V. R. Hentz, "Quantification of fingertip force reduction in the forefinger following simulated paralysis of extensor and intrinsic muscles," *Journal of Biomechanics*, vol. 33, no. 12, pp. 1601 – 1609, 2000.

[16] C. M. Niu, S. Nandyala, W. J. Sohn, and T. Sanger, "Multi-scale hyper-time hardware emulation of human motor nervous system based on spiking neurons using fpga," in *Advances in Neural Information Processing Systems*, pp. 37–45, 2012.

[17] M. P. Mileusnic, I. E. Brown, N. Lan, and G. E. Loeb, "Mathematical models of proprioceptors. i. control and transduction in the muscle spindle," *Journal of neurophysiology*, vol. 96, no. 4, pp. 1772–1788, 2006.

[18] B. B. Edin and A. Vallbo, "Dynamic response of human muscle spindle afferents to stretch," *Journal of Neurophysiology*, vol. 63, no. 6, pp. 1297–1306, 1990.

[19] A. Jobin and M. F. Levin, "Regulation of stretch reflex threshold in elbow flexors in children with cerebral palsy: a new measure of spasticity," *Developmental Medicine & Child Neurology*, vol. 42, no. 8, pp. 531–540, 2000.

[20] D. G. Kamper and W. Z. Rymer, "Quantitative features of the stretch response of extrinsic finger muscles in hemiparetic stroke," *Muscle & nerve*, vol. 23, no. 6, pp. 954–961, 2000.

[21] A. R. Radulescu, "Mechanisms explaining transitions between tonic and phasic firing in neuronal populations as predicted by a low dimensional firing rate model," *PloS one*, vol. 5, no. 9,

$\mathcal{L\!\!}^{A}T_{\!E}X\,2_{\varepsilon}$                                                                                                22

p. e12695, 2010.

[22] E. Toft, T. Sinkjaer, S. Andreassen, and K. Larsen, "Mechanical and electromyographic responses to stretch of the human ankle extensors," *Journal of Neurophysiology*, vol. 65, no. 6, pp. 1402–1410, 1991.

[23] R. Powers, D. Campbell, and W. Rymer, "Stretch reflex dynamics in spastic elbow flexor muscles," *Annals of neurology*, vol. 25, no. 1, pp. 32–42, 1989.

[24] C. Larivière, D. Ludvig, R. Kearney, H. Mecheri, J.-M. Caron, and R. Preuss, "Identification of intrinsic and reflexive contributions to low-back stiffness: medium-term reliability and construct validity," *Journal of Biomechanics*, vol. 48, no. 2, pp. 254 – 261, 2015.

[25] M. M. Mirbagheri, L. Alibiglou, M. Thajchayapong, and W. Z. Rymer, "Muscle and reflex changes with varying joint angle in hemiparetic stroke," *Journal of neuroengineering and rehabilitation*, vol. 5, no. 1, p. 1, 2008.

[26] A. F. d. C. Hamilton, K. E. Jones, and D. M. Wolpert, "The scaling of motor noise with muscle strength and motor unit number in humans," *Experimental Brain Research*, vol. 157, no. 4, pp. 417–430, 2004.

[27] R. M. Enoka, R. A. Burnett, A. E. Graves, K. W. Kornatz, and D. H. Laidlaw, "Task-and age-dependent variations in steadiness," *Progress in brain research*, vol. 123, pp. 389–395, 1999.

[28] K. E. Jones, A. F. d. C. Hamilton, and D. M. Wolpert, "Sources of signal-dependent noise during isometric force production," *Journal of neurophysiology*, vol. 88, no. 3, pp. 1533–1544, 2002.

[29] R. B. Stein and C. Capaday, "The modulation of human reflexes during functional motor tasks," *Trends in neurosciences*, vol. 11, no. 7, pp. 328–332, 1988.

[30] M. M. Mirbagheri, H. Barbeau, and R. E. Kearney, "Intrinsic and reflex contributions to human ankle stiffness: variation with activation level and position," *Experimental Brain Research*, vol. 135, no. 4, pp. 423–436, 2000.

[31] M. Sreenivasa, K. Ayusawa, and Y. Nakamura, "Modeling and identification of a realistic spiking neural network and musculoskeletal model of the human arm, and an application to the stretch reflex," *IEEE Transactions on Neural Systems and Rehabilitation Engineering*, vol. 24, no. 5, pp. 591–602, 2016.

[32] J. J. Kutch and F. J. Valero-Cuevas, "Challenges and new approaches to proving the existence of muscle synergies of neural origin," *PLoS Comput. Biol*, vol. 8, no. 5, 2012.

[33] M. U. Kurse, H. Lipson, and F. J. Valero-Cuevas, "Extrapolatable analytical functions for tendon excursions and moment arms from sparse datasets," *Biomedical Engineering, IEEE Transactions on*, vol. 59, no. 6, pp. 1572–1582, 2012.

[34] F. J. Valero-Cuevas, H. Hoffmann, M. U. Kurse, J. J. Kutch, and E. A. Theodorou, "Computational models for neuromuscular function," *Biomedical Engineering, IEEE Reviews in*, vol. 2, pp. 110–135, 2009.

[35] M. P. Mileusnic and G. E. Loeb, "Mathematical models of proprioceptors. ii. structure and function of the golgi tendon organ," *Journal of Neurophysiology*, vol. 96, no. 4, pp. 1789–1802, 2006.

[36] M. Dimitriou, "Human muscle spindle sensitivity reflects the balance of activity between antagonistic muscles," *The Journal of Neuroscience*, vol. 34, no. 41, pp. 13644–13655, 2014.

[37] E. Glowatzki and P. A. Fuchs, "Transmitter release at the hair cell ribbon synapse," *Nature neuroscience*, vol. 5, no. 2, pp. 147–154, 2002.

[38] B. J. Schmidt and L. M. Jordan, "The role of serotonin in reflex modulation and locomotor rhythm production in the mammalian spinal cord," *Brain research bulletin*, vol. 53, no. 5, pp. 689–710, 2000.

[39] S. Grillner, "The motor infrastructure: from ion channels to neuronal networks," *Nature Reviews Neuroscience*, vol. 4, no. 7, pp. 573–586, 2003.

[40] A. J. Fuglevand, D. A. Winter, and A. E. Patla, "Models of recruitment and rate coding organization in motor-unit pools," *Journal of neurophysiology*, vol. 70, no. 6, pp. 2470–2488, 1993.

[41] R. Shadmehr and S. P. Wise, *The computational neurobiology of reaching and pointing: a*

$\mathcal{L\!A\!T\!E\!X}\,2_\varepsilon$                                                                        23

*foundation for motor learning*. MIT press, 2005.

[42] F. E. Zajac, "How musculotendon architecture and joint geometry affect the capacity of muscles to move and exert force on objects: a review with application to arm and forearm tendon transfer design," *The Journal of hand surgery*, vol. 17, no. 5, pp. 799–804, 1992.

[43] C. M. Laine, A. Nagamori, and F. J. Valero-Cuevas, "The dynamics of voluntary force production in afferented muscle influence involuntary tremor," *Frontiers in Computational Neuroscience*, vol. 10, no. 86, 2016.

[44] C. M. Laine, E. Martinez-Valdes, D. Falla, F. Mayer, and D. Farina, "Motor neuron pools of synergistic thigh muscles share most of their synaptic input," *The Journal of Neuroscience*, vol. 35, no. 35, pp. 12207–12216, 2015.

[45] C. Laine, Ş. Yavuz, and D. Farina, "Task-related changes in sensorimotor integration influence the common synaptic input to motor neurones," *Acta Physiologica*, vol. 211, no. 1, pp. 229–239, 2014.

[46] T. W. Boonstra, "The potential of corticomuscular and intermuscular coherence for research on human motor control," *Frontiers in human neuroscience*, vol. 7, 2013.

[47] R. W. Bohannon and M. B. Smith, "Interrater reliability of a modified ashworth scale of muscle spasticity," *Physical therapy*, vol. 67, no. 2, pp. 206–207, 1987.

[48] E. J. Cheng, I. E. Brown, and G. E. Loeb, "Virtual muscle: a computational approach to understanding the effects of muscle properties on motor control," *Journal of neuroscience methods*, vol. 101, no. 2, pp. 117–130, 2000.

[49] K. Jalaleddini, T. E. Sobhani, and R. Kearney, "A subspace approach to the structural decomposition and identification of ankle joint dynamic stiffness," *IEEE transactions on biomedical engineering*, 2016.

[50] F. Valero-Cuevas and H. Lipson, "A computational environment to simulate complex tendinous topologies," in *Engineering in Medicine and Biology Society, 2004. IEMBS'04. 26th Annual International Conference of the IEEE*, vol. 2, pp. 4653–4656, IEEE, 2004.

[51] F. J. Valero-Cuevas, *Fundamentals of Neuromechanics*. Springer, 2016.

[52] J. M. Inouye and F. J. Valero-Cuevas, "Muscle synergies heavily influence the neural control of arm endpoint stiffness and energy consumption," *PLoS Comput Biol*, vol. 12, no. 2, p. e1004737, 2016.

[53] F. Valero-Cuevas, B. Cohn, H. Yngvason, and E. Lawrence, "Exploring the high-dimensional structure of muscle redundancy via subject-specific and generic musculoskeletal models," *Journal of biomechanics*, 2015.

[54] K. G. Keenan, V. J. Santos, M. Venkadesan, and F. J. Valero-Cuevas, "Maximal voluntary fingertip force production is not limited by movement speed in combined motion and force tasks," *The Journal of Neuroscience*, vol. 29, no. 27, pp. 8784–8789, 2009.

[55] Å. Vallbo, "Discharge patterns in human muscle spindle afferents during isometric voluntary contractions," *Acta Physiologica Scandinavica*, vol. 80, no. 4, pp. 552–566, 1970.

[56] C. S. Sherrington, "Reflex inhibition as a factor in the co-ordination of movements and postures," *Quarterly Journal of Experimental Physiology*, vol. 6, no. 3, pp. 251–310, 1913.

[57] G. Raphael, G. A. Tsianos, and G. E. Loeb, "Spinal-like regulator facilitates control of a two-degree-of-freedom wrist," *The Journal of Neuroscience*, vol. 30, no. 28, pp. 9431–9444, 2010.

[58] T. D. Sanger, D. Chen, D. L. Fehlings, M. Hallett, A. E. Lang, J. W. Mink, H. S. Singer, K. Alter, H. Ben-Pazi, E. E. Butler, *et al.*, "Definition and classification of hyperkinetic movements in childhood," *Movement Disorders*, vol. 25, no. 11, pp. 1538–1549, 2010.

[59] V. R. Hentz and C. Leclercq, *Surgical rehabilitation of the upper limb in tetraplegia*. WB Saunders London, 2002.

[60] E. L. Air, J. L. Ostrem, T. D. Sanger, and P. A. Starr, "Deep brain stimulation in children: experience and technical pearls: Clinical article," *Journal of Neurosurgery: Pediatrics*, vol. 8, no. 6, pp. 566–574, 2011.

[61] H. B. Hayes, A. Jayaraman, M. Herrmann, G. S. Mitchell, W. Z. Rymer, and R. D. Trumbower,

$\mathit{L\!A\!T\!E\!X\,2_\varepsilon}$                                                                    24

"Daily intermittent hypoxia enhances walking after chronic spinal cord injury a randomized trial," *Neurology*, vol. 82, no. 2, pp. 104–113, 2014.